

Critical role of friction for a single particle falling through a funnel

Qiang Zhang, Yuan Fang, and Jonathan J. Wylie

Department of Mathematics, City University of Hong Kong, Kowloon, Hong Kong

(Received 22 September 2010; revised manuscript received 12 March 2011; published 12 May 2011)

We investigate a single frictional, inelastic, spherical particle falling under gravity through a symmetric funnel. A recent study showed that, for a frictionless particle in such a system, several anomalous phenomena occur: The particle can stay longer, lose more energy, and exert more impulsive force in a funnel with steeper walls. For frictionless particles, such phenomena exist for many small ranges of funnel angles and are a consequence of the many possible repeated patterns in particle trajectories. However, in reality, friction always exists and it is a natural question whether the anomalous phenomena still exist for frictional particles in such systems. We show that, surprisingly, the inclusion of friction in the dynamics actually dramatically enhances the anomalous phenomena. For frictional particles, the anomalous phenomena exist for all funnel angles steeper than 45° and are thus more robust than the frictionless case. Furthermore, instead of many possible complicated repeated patterns in particle trajectories, there is a unique repeated pattern for frictional particles. Moreover, this is the simplest possible repeated pattern. We derive an analytical expression for this unique repeated pattern and provide a theoretical explanation for the anomalous phenomena observed in frictional particle systems. We further show that the friction, no matter how small, plays a critical role in the dynamics, that is, the dynamics of the frictionless particle system is singular.

DOI: [10.1103/PhysRevE.83.051303](https://doi.org/10.1103/PhysRevE.83.051303)

PACS number(s): 81.05.Rm, 45.50.-j

I. INTRODUCTION

In this paper we consider a system in which a single inelastic frictional particle with uniform density falls under gravity through a symmetric funnel. A recent study of a frictionless particle falling through a funnel showed several surprising results [1]. Counterintuitively, the study showed that there are several small ranges of funnel angle where the particle will fall through funnels with less steep sides more quickly, exert a smaller total impulse on the funnel walls, and lose less energy. This counterintuitive behavior exists due to the existence of repeated patterns in the particle trajectories. Stability analysis of these trajectories shows that the anomalous phenomena can occur only in narrow ranges of funnel angles. However, in general, particles are always frictional. Friction leads to particle rotation, which does not occur in the frictionless case. This rotation makes the dynamics more complicated and may destroy the repeated patterns. This raises an important question of whether such an anomalous phenomenon still exists in systems with frictional particles. In this paper we show that the friction not only preserves the anomalous phenomenon, but also enhances it considerably. In particular, due to the effects of friction, we show that the average time the particles stay in the funnel is anomalously long for funnels with walls inclined at angles greater than 45° to the horizontal. This is in direct contrast to the frictionless case in which the anomalous behavior occurs only in narrow angular ranges. Moreover, there is a unique repeated pattern instead of the large number of complicated repeated patterns observed in the frictionless case.

Funnel systems are widespread in many industrial devices in which falling particles must be steered into a thin slot or hole. Depending on the particular application, the fulfillment of different design objectives may be required. Examples include minimizing the duration that particles spend in the device, reducing the machine wear, or reducing the speed of particles exiting the machine. In this paper we show that an

apparently simple system has a number of complicated and subtle features that make the achievement of design objectives highly counterintuitive.

The behavior of dense granular flow through funnels has been widely studied and a number of important results have been obtained. Schick and Verveen [2] studied dense flow through an hourglass and made detailed observations of the noise in such systems. Baxter *et al.* [3] studied dense flow through a funnel and found that the formation and propagation of density waves depend on the mass flow rate and geometry of the funnel. Wu *et al.* [4] and Veje and Dimon [5] considered dense flows in a closed-top hourglass and found that the counterflow of air can induce surprising dynamics such as oscillatory behavior and cluster formation. Veje and Dimon [6] considered a dense flow consisting of a single layer of uniform balls and showed that the geometry of the funnel can have a strong effect on the resulting flow patterns. Moriyama *et al.* [7] performed careful experiments of sand flowing through a vertical pipe and were able to determine the form of the density variations in such systems. Le Pennec *et al.* [8] studied two-dimensional dense funnel flow and determined how the flow depends on the geometry of the funnel. Longhi *et al.* [9] studied the force fluctuations at the boundary of a two-dimensional dense granular flow and determined the distribution of impulses. Horlück *et al.* [10] investigated the effects of rough walls and polydispersity on shock waves in two-dimensional granular flow. Helbing *et al.* [11] proposed a continuum model for dense granular flow through a funnel that explains a number of important features of funnel flow including intermittency.

Surprisingly, in the funnel setting, the case of dilute flows that contain a small number of particles or even only a single particle (such as the study in this paper) has received much less attention. In other settings, studies of this type of system have led to important insights into the way in which granular materials behave. Mehta and Luck [12,13] showed

that a single particle moving under gravity on a vibrating plate can give rise to highly unexpected behavior such as abrupt termination of period-doubling sequences. McNamara and Young [14] showed that a finite number of particles is required to obtain an infinite number of collisions in a finite time. Wylie and co-workers [15,16] investigated the dynamical behavior of a one-dimensional inelastic particle system with particles of unequal mass traveling between two walls and showed that two driven inelastic particles can experience a bifurcation in which large numbers of complicated periodic orbits collapse onto a single simple orbit. Gao *et al.* [17] studied the collapse phenomena when a rigid, frictionless, inelastic particle interacts with a rigid boundary that has a corner.

To study the dynamics of frictional granular particles falling through a funnel, one needs to specify a model for collisions between particles and funnel walls. Such a model has been developed by Walton [18]. The model is based on three constant impact coefficients, which are the coefficient of normal restitution, the coefficient of friction, and the coefficient of tangential restitution. Foerster *et al.* [19] carried out experiments to measure the collision properties of small spheres involved in binary collisions or in collisions with a flat surface and showed that Walton's model [18] provides an accurate description of the dynamics of the impacts. Luding [20] simulated two-dimensional systems of spheres in a vibrating box using Walton's model [18] and found that the behavior of the system depends on the frictional properties of both particles and walls and presented an expression for the ratio of kinetic to rotational energy. In Ref. [21], Brilliantov *et al.* proposed a collision model in which the restitution coefficients for the normal and tangential motion can be calculated as functions of the impact velocity from considerations of dissipative viscoelastic collisions. In this paper we will adopt the model used in Refs. [18–20].

The rest of the paper is organized as follows. In Sec. II we present the theoretical formulation for the system of a frictional, inelastic particle falling through a symmetric funnel. In Sec. III we demonstrate numerically the counterintuitive phenomena in frictional particle systems. In Sec. IV we provide a theoretical explanation for the anomalous phenomena in such systems. In Sec. V we examine three-dimensional systems with an axisymmetric conical funnel. Finally, we summarize in Sec. VI.

II. FORMULATION

In this paper we consider a frictional, inelastic particle of radius a with uniform density, falling under gravity g through a symmetric funnel with walls aligned at an angle θ to the horizontal and a gap of size d at the bottom of the funnel. The particle is released with zero initial velocity and zero initial angular velocity with its center at a height H above the bottom of the funnel and at a horizontal location x_0 measured from the central axis of the funnel (see Fig. 1). A particle will experience collisions with the walls when the center of the particle is a distance a from the wall. It thus proves convenient to consider the lines that are parallel to the walls and a distance a from the walls. We choose the origin of coordinates to be the point where these lines intersect. We choose the x axis to be

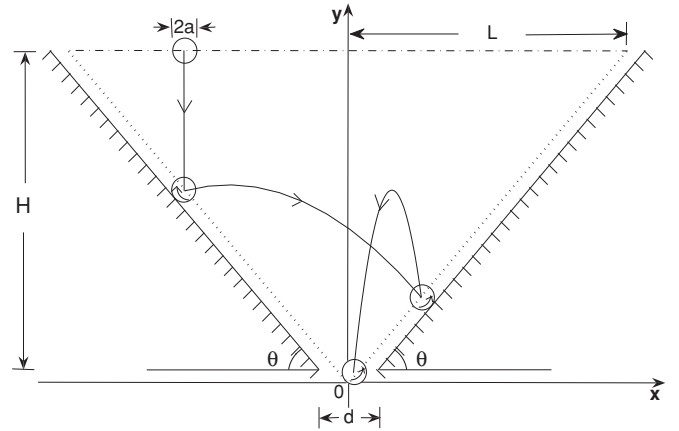


FIG. 1. Sketch of a system in which a frictional particle falls through a funnel with an angle θ . The dash-dotted horizontal line represents the range over which the center of the particle lies when the particle is released. The dotted lines are parallel to the funnel walls at a distance a from the walls. We choose the origin of coordinates to be the point where the two dotted lines intersect.

horizontal and the y axis to be vertically upward (see Fig. 1). We nondimensionalize lengths by H , times by $\sqrt{H/g}$, and velocities by \sqrt{Hg} .

We will consider the case where particles are dropped into the funnel at a random horizontal location x_0 . For simplicity, we will consider the probability density function that is uniform for all values of x_0 . We note that other choices of probability density functions give qualitatively similar results.

The trajectory of a particle is determined by a sequence of collisions of the particle with the walls and free-fall motion under gravity between the collisions. Determination of the sequence in which collisions occur is a nonlinear process and we show that this can lead to complicated behavior.

We begin by discussing the nature of the collisions. When the particle collides with the wall, the particle experiences an impulsive force from the wall. We determine the dynamics of the particle by considering rigid-body motion under an impulsive collisional force. Rigid-body motion is composed of two parts: the motion of the center of mass and the rotation of the body around the center of mass. The description of the collision between the particle and the wall is based on the collision model introduced by Walton [18] and studied in detail by Foerster *et al.* [19] and Luding [20].

We will assume that collisions between the particle and the wall are inelastic with a constant coefficient of restitution e , that is,

$$p' = -ep, \quad (1)$$

where p and p' are the velocity components perpendicular to the wall, before and after the collision, respectively. The change of translational momentum in the direction perpendicular to the wall is given by

$$m(p' - p) = J_N, \quad (2)$$

where J_N is the component of the impulse exerted on the particle perpendicular to the wall. Using Eq. (1), we obtain

$$-m(1+e)p = J_N. \quad (3)$$

The change of momentum in the direction parallel to the wall before and after a collision is given by

$$m(q' - q) = J_t, \quad (4)$$

where q and q' are the velocity components tangential to the wall, before and after a collision respectively, and J_t is the component of the impulse exerted on the particle parallel to the wall. The change in angular momentum due to the collision is given by

$$I(\omega' - \omega) = aJ_t, \quad (5)$$

where I is the moment of inertia and ω and ω' are the angular velocities before and after the collision, respectively.

When the relative velocity between the particle and the boundary is nonzero, i.e., the collision involves sliding, the tangential and normal components of the impulse are related by Coulomb's law, that is, $|J_t| = \mu|J_N|$, with the coefficient of sliding friction $\mu \geq 0$, which is assumed to be a constant in this paper. The direction of J_t is opposite the tangential velocity at the contact point before the collision, $q + a\omega$, because the contact is dissipative, i.e.,

$$J_t = -\mu m(1+e)s|p|, \quad (6)$$

where the quantity s is the sign of the particle's tangential velocity along the wall surface immediately before contact. On the left wall, we define the downward direction along the wall as being positive, so that $s = 1, -1$, and 0 when the tangential velocity at the point of contact is downward, upward, or zero, respectively. On the right wall, we define the upward direction along the wall as the positive direction, so that $s = 1, -1$, and 0 when the velocity at the point of contact is upward, downward, or zero, respectively.

If one substitutes Eq. (6) into Eqs. (4) and (5), the magnitude of the tangential velocity at the contact point right after the collision, $|q' + a\omega'|$, can be greater than $|q + a\omega|$ in the case of sufficiently large μ . To avoid this problem, Walton [18] introduced the coefficient of maximum tangential restitution β_0 , with $-1 \leq \beta_0 \leq 1$. As $|J_t|$ increases, sliding is deemed to cease when

$$q' + a\omega' = -\beta_0(q + a\omega). \quad (7)$$

For given p , q , and ω , we can determine a critical value of the friction, μ_c , so that, for values of $\mu \geq \mu_c$, the collision does not involve sliding; namely, from Eqs. (4)–(7), we obtain

$$\mu_c = \frac{(1 + \beta_0)|q + a\omega|}{(1 + e)\left(\frac{ma^2}{I} + 1\right)|p|}.$$

In Coulomb-type contacts [18], i.e., $\mu < \mu_c$, the tangential velocity of the center of mass after a collision is determined by Eqs. (4) and (6),

$$q' = q - \mu(1+e)|p|s, \quad (8)$$

and the postcollisional angular velocity can be obtained from Eqs. (5) and (6),

$$\omega' = \omega - \frac{\mu(1+e)|p|sma}{I}. \quad (9)$$

In the case $\mu \geq \mu_c$, Eqs. (4), (5), and (7) give

$$q' = \frac{ma^2 - I\beta_0}{I + ma^2}q - \frac{Ia}{I + ma^2}(1 + \beta_0)\omega, \quad (10)$$

$$\omega' = -\frac{q' + \beta_0(q + a\omega)}{a} = -\frac{ma(1 + \beta_0)}{I + ma^2}q + \frac{I - ma^2\beta_0}{I + ma^2}\omega. \quad (11)$$

We now calculate the energy loss during each collision. We need to consider two cases: $\mu < \mu_c$ and $\mu > \mu_c$. When $\mu < \mu_c$, the velocity and angular velocity after the collision are determined by Eqs. (1), (8), and (9) and the energy loss is

$$\begin{aligned} \Delta E_1 &= \frac{1}{2}m(q^2 - q'^2) + \frac{1}{2}m(p^2 - p'^2) + \frac{1}{2}I(\omega^2 - \omega'^2) \\ &= \frac{1}{2}m(1 - e^2)p^2 + \frac{1}{2}m\mu(1 + e) \\ &\quad \times |p(q + a\omega)| \left(2 - \frac{\mu(1 + \beta_0)}{\mu_c}\right). \end{aligned}$$

Note that $\mu < \mu_c$ and therefore if $\mu \neq 0$ and $e \neq 1$, any collision must involve energy loss. When μ exceeds μ_c , the velocity and angular velocity after the collision are determined by Eqs. (1), (10), and (11), so we obtain the energy loss

$$\begin{aligned} \Delta E_2 &= \frac{1}{2}m(q^2 - q'^2) + \frac{1}{2}m(p^2 - p'^2) + \frac{1}{2}I(\omega^2 - \omega'^2) \\ &= \frac{1}{2}m(1 - e^2)p^2 + \frac{1}{2} \frac{mI(1 - \beta_0^2)}{I + ma^2}(q + a\omega)^2. \end{aligned}$$

In this case the energy loss is independent of μ . Note that when $\mu = \mu_c$, $\Delta E_1 = \Delta E_2$. It is easy to see that $\Delta E_2 = 0$ if and only if $e = 1$ and

$$a\omega + q = 0 \quad \text{or} \quad |\beta_0| = 1. \quad (12)$$

Therefore, the energy is conserved for an elastic particle whose tangential velocity of the contact point before collision is zero or $\beta_0 = \pm 1$.

Between collisions, the particle experiences free-fall motion and so the trajectory of the particle follows a parabolic curve. The next collision point is determined by one of three possible events: The particle collides with the left funnel wall, it collides with the right funnel wall, or it exits the funnel through the gap. One needs to determine which of the three events occurs first. This makes determining explicit expressions for the motion extremely difficult. However, the motion can be easily determined numerically for a given trajectory.

The phenomenon of inelastic collapse may occur, in which the particle may experience an infinite number of collisions with one of the walls in a finite time. It is easy to handle inelastic collapse since the time of inelastic collapse can be determined analytically. After the collapse, the particle will roll down along one of the walls.

We will also study frictional particles falling through an axisymmetric conical funnel. We note that the trajectory of

a particle in a two-dimensional funnel and the trajectory of a particle in an axisymmetric conical funnel are identical if the particle is released at the same distance from the axis of symmetry with zero initial velocity. However, if the initial particle locations are assumed to be uniformly distributed, then the averages in the two cases must be computed with respect to different distributions. We will return to this issue in Sec. V, where we show that the qualitative behavior is similar in both cases.

III. COUNTERINTUITIVE PHENOMENA

The algorithm described in the preceding section allows us to perform detailed numerical simulations of the complicated nonlinear dynamical behavior of particles falling through a funnel. In this section we demonstrate some counterintuitive phenomena in such simple systems. We set $a/H = 0.01$ and $d/H = 0.04$ in our simulations. For given values of e , μ , β_0 , and θ , we simulate 4000 sample trajectories with uniformly spaced initial horizontal locations x_0 . For each x_0 , we record the duration that the particle stays in the funnel.

Figure 2 shows the duration that the particle stays in the funnel averaged over the horizontal release position as a function of θ for the different values of e in the frictionless case that was studied in Ref. [1]. The overall trend for each of the curves is that the average duration decreases with the angle of the funnel. This is consistent with our intuition: A particle will spend less time in a steeper funnel. However, counterintuitively, there exist ranges of angles such that the particle will stay longer in a funnel with a steeper angle. Fang *et al.* [1] showed that such anomalous behavior in these ranges of angles is due to the existence of some neutrally stable quasiperiodic orbits in which the particle collisions follow a simple repeating pattern. These simple repeating collision patterns can imply that the particle can stay far from the exit for long periods of time. Outside these ranges of angles the particle collisions follow a complicated nonrepeating pattern and the particle rapidly hits the exit. As e gets smaller, particles lose more energy per collision and the collision locations move

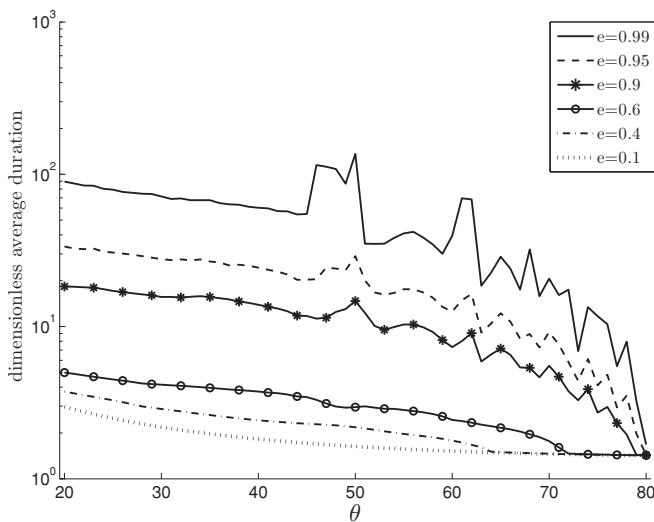


FIG. 2. Average duration (nondimensionalized by $\sqrt{H/g}$) plotted against θ for frictionless systems with different values of e .

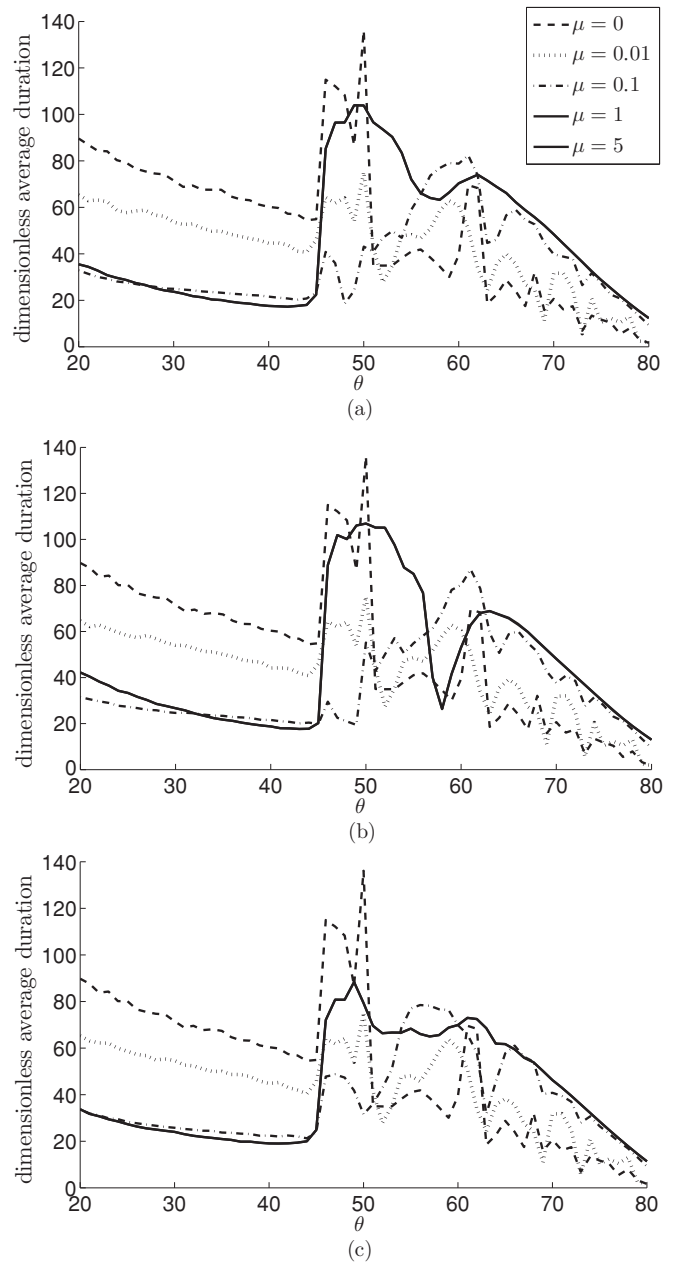


FIG. 3. Average duration (nondimensionalized by $\sqrt{H/g}$) plotted against θ for systems with $e = 0.99$ and various values of μ for (a) $\beta_0 = 0$, (b) $\beta_0 = 0.31$, and (c) $\beta_0 = -0.31$. The curves with $\mu = 1$ and those with $\mu = 5$ almost coincide.

down toward the exit more quickly. Consequently, even the simple orbits will stay a relatively short time in the funnel; therefore, the jumps become less pronounced as e decreases.

In Fig. 3 we show how friction affects the anomalous behavior observed in frictionless systems. We plot the average duration with $e = 0.99$ and different values of μ for three different values of β_0 . Figure 3(a) shows the case for $\beta_0 = 0$; Fig. 3(b) shows the case for $\beta_0 = 0.31$, which is suggested by the experiments of Ref. [19]; and β_0 can be negative [20], so we plot the case for $\beta_0 = -0.31$ in Fig. 3(c). In the absence of friction ($\mu = 0$), the particle does not rotate. The presence of friction allows the particle to rotate. This rotation means that the motion of the particle has an extra degree of

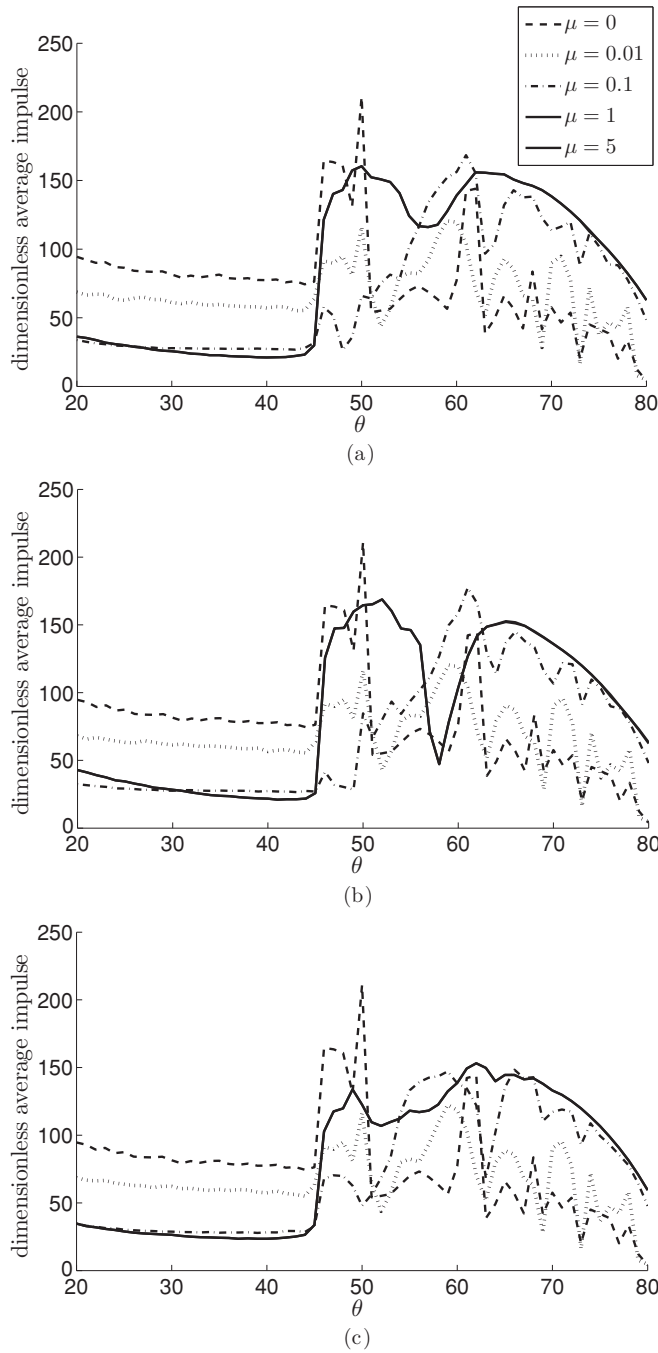


FIG. 4. Average impulse (nondimensionalized by $m\sqrt{gH}$) plotted against θ for systems with $e = 0.99$ and various values of μ for (a) $\beta_0 = 0$, (b) $\beta_0 = 0.31$, and (c) $\beta_0 = -0.31$. The curves with $\mu = 1$ and those with $\mu = 5$ almost coincide.

freedom. In general, the higher the degree of freedom, the more complicated the trajectory can be. Consequently, one might imagine that simple repeating patterns of collisions will be less likely and so particles will have more of a chance to hit the exit of the funnel earlier. This will lead to shortening the average duration that particles stay inside the funnel. This is indeed the case for $\theta < 45^\circ$. Figure 3 shows that the average duration is a decreasing function of μ and θ when $\theta < 45^\circ$. Therefore, the steeper the funnel wall, or the larger the friction, the shorter the average duration is. This is consistent with our

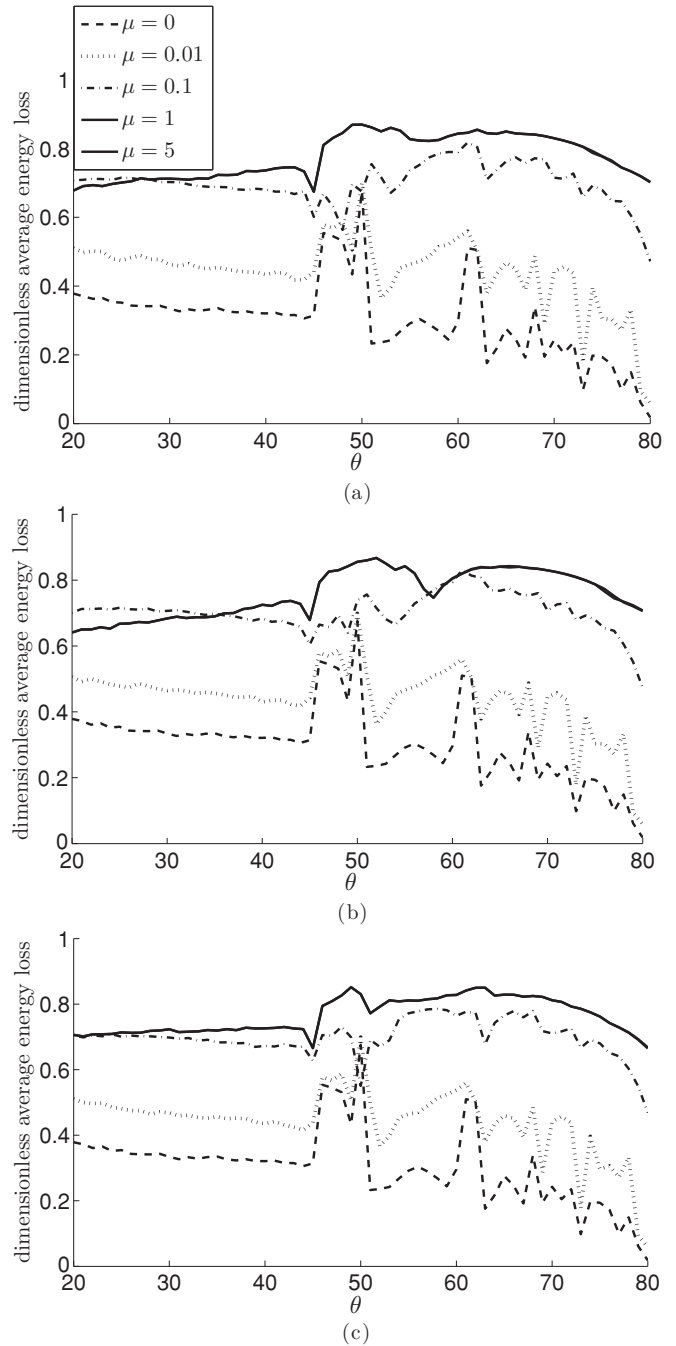


FIG. 5. Average energy loss (nondimensionalized by mgH) plotted against θ for systems with $e = 0.99$ and various values of μ for (a) $\beta_0 = 0$, (b) $\beta_0 = 0.31$, and (c) $\beta_0 = -0.31$. The curves with $\mu = 1$ and those with $\mu = 5$ almost coincide.

intuition. However, the effect of friction on duration is very different for $\theta > 45^\circ$. Figure 3 shows that the range of angles θ over which the average duration is larger than that in a funnel with $\theta = 45^\circ$ widens as μ increases. For large values of μ , almost all angles in the range $\theta > 45^\circ$ have an average duration longer than that at $\theta = 45^\circ$.

In industrial applications, the impulse exerted on the walls is an important quantity for understanding machine wear. In Fig. 4 we show the average impulse as a function of θ for different values of μ when $e = 0.99$ for the same

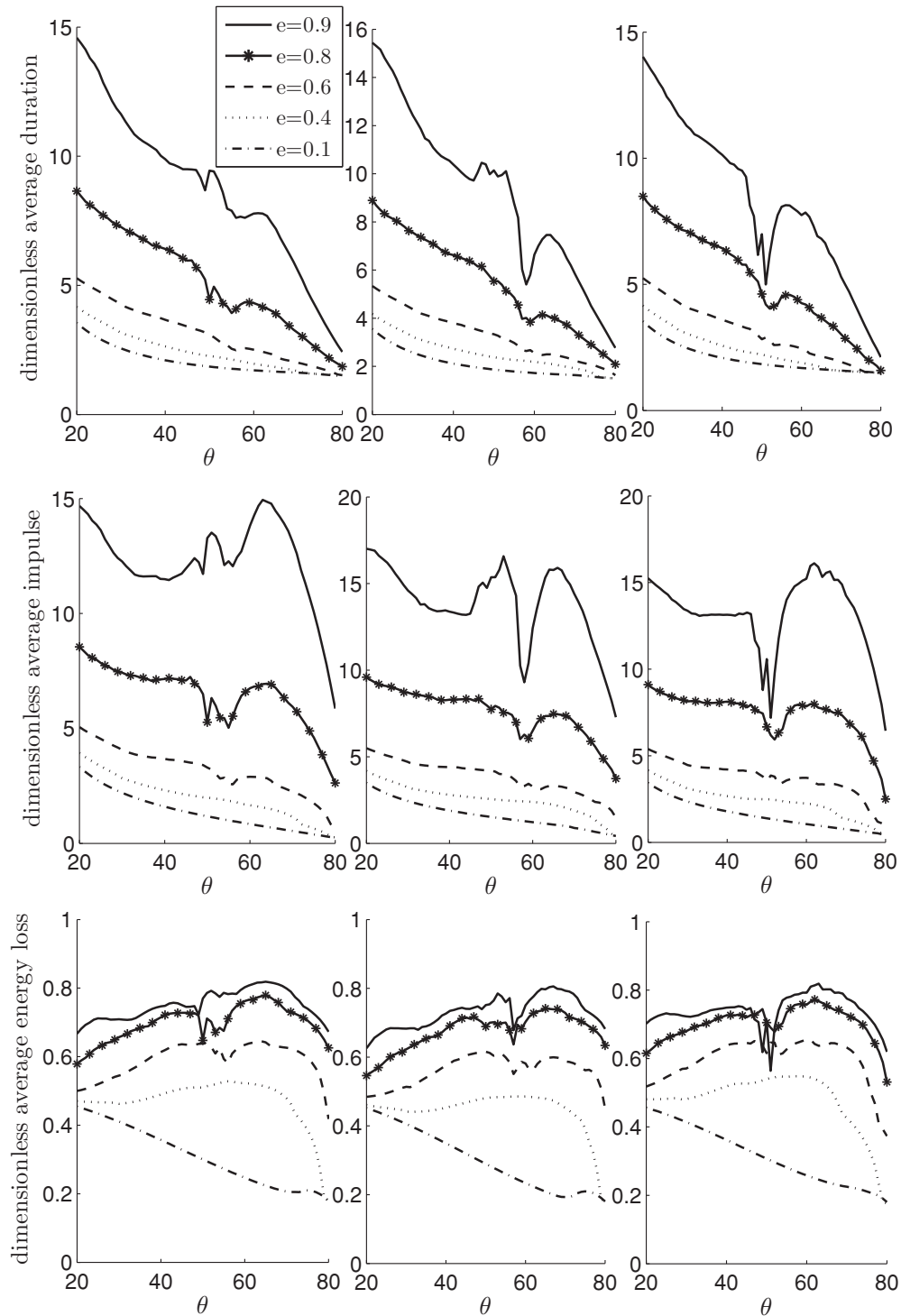


FIG. 6. Average duration (nondimensionalized by $\sqrt{H/g}$), impulse (nondimensionalized by $m\sqrt{gH}$), and energy loss (nondimensionalized by mgH) plotted against θ for systems with $\mu = 1$ and different values of e . From left to right, the plots correspond to $\beta_0 = 0, 0.31,$ and -0.31 respectively.

values of β_0 as in Fig. 3. The behavior for the average total impulse is shown to be very similar to the behavior for the average duration shown in Fig. 3, namely, for fixed $\theta < 45^\circ$, the average impulse decreases with μ and θ . This is consistent with our intuition: The shorter the particle stays inside the funnel, the fewer collisions it has with the wall

and consequently the smaller impulse it exerts. However, the situation is very different for $\theta > 45^\circ$. When μ is large, almost all funnels with $\theta > 45^\circ$ experience a larger average impulse than the funnel with $\theta = 45^\circ$. Although such behavior is counterintuitive, it is consistent with the phenomenon shown in Fig. 3.

When the particle collides with the funnel boundaries, it loses energy due to two factors: inelastic collisions and friction. Figure 5 shows the average energy loss when the particle exits the funnel. Generally speaking, the particle loses more energy as friction increases until μ reaches a critical value; when μ exceeds this critical value, the energy loss is independent of μ .

We also plot the average duration, impulse, and energy loss in the systems with large μ and various values of e in Fig. 6. From left to right, the plots correspond to $\beta_0 = 0, 0.31,$ and $-0.31,$ respectively. We can see that as e becomes smaller, the anomalous phenomenon becomes less pronounced. However, from the figures of average impulse and energy loss, we can observe that the behaviors in the systems with $\theta < 45^\circ$ and $\theta > 45^\circ$ are still very different, even for moderate values of e . For sufficiently small values of e ($e = 0.4$ and 0.1), we can see that the average duration is almost monotonic. This is because, when e is small, most particles do not have enough energy to jump to the other wall and instead collide with only one of the walls; the velocity component perpendicular to the wall will be damped quickly and the particles just roll down along the wall. Since the behavior for small e is quite intuitive and natural, we will mainly focus on the counter-intuitive behavior that occurs for particles with e close to unity.

We therefore examine further the dynamics of funnels with $e = 0.99$ and a relatively large value of μ . To understand the quite different behavior between the funnels with $\theta < 45^\circ$ and those with $\theta > 45^\circ$, we demonstrate the duration spent in the funnel as a function of the scaled input location x_0/L for funnels with various values of θ for the case of $\beta_0 = 0$ (see Fig. 7). Here L is half the effective opening of the funnel for the center of the particle and is marked on Fig. 1. The behavior of duration for other values of β_0 is very similar to that shown in Fig. 7. Figures 7(a)–7(d) show that when $\theta < 45^\circ$, the duration is highly sensitive to the initial location x_0 , while Figs. 7(e)–7(i) show that for $\theta > 45^\circ$, there are ranges of initial locations where the duration is relatively insensitive to the initial location. Figures 7(d) and 7(e) show that, even when θ changes only from 44° to 46° , the sensitivity to the initial location changes dramatically. We now examine the trajectories in these insensitive ranges. Figure 8(a) shows a typical trajectory for $\theta > 45^\circ$. After a certain number of collisions, the trajectory starts to follow a simple repeating pattern of collisions: bouncing back and forth between the left and right walls while slowly falling down through the funnel toward the exit. Our simulations showed that this pattern of collisions is observed only in Figs. 7(e)–7(i), which all have $\theta > 45^\circ$, but not in Figs. 7(a)–7(d), which all have $\theta < 45^\circ$. In contrast, Fig. 8(b) is a typical trajectory, observed

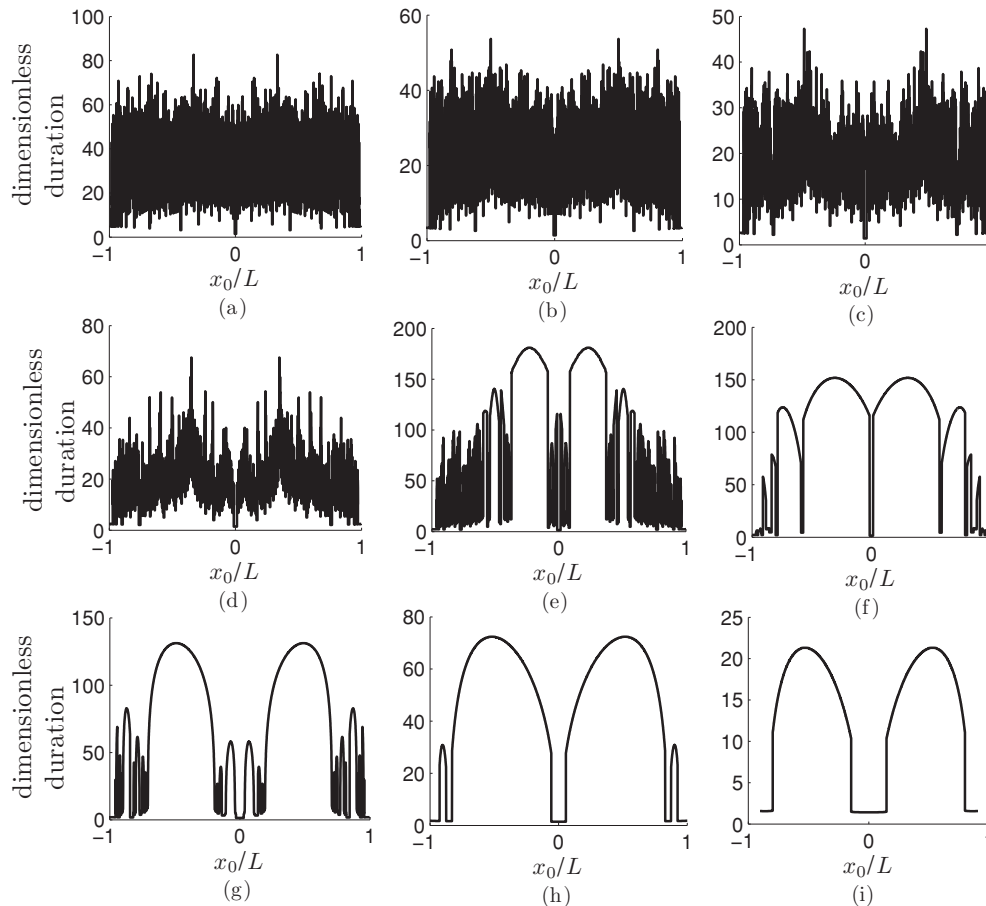


FIG. 7. Duration (nondimensionalized by $\sqrt{H/g}$) plotted against the scaled initial location x_0/L for funnels with (a) $\theta = 20^\circ$, (b) $\theta = 30^\circ$, (c) $\theta = 40^\circ$, (d) $\theta = 44^\circ$, (e) $\theta = 46^\circ$, (f) $\theta = 50^\circ$, (g) $\theta = 60^\circ$, (h) $\theta = 70^\circ$, and (i) $\theta = 80^\circ$. Here $e = 0.99, \mu = 1, \beta_0 = 0,$ and L is half the effective opening of the funnel for the center of the particle (see Fig. 1).

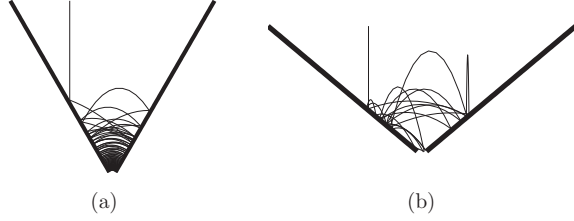


FIG. 8. Particle trajectories for funnels with (a) $\theta = 60^\circ$ and (b) $\theta = 40^\circ$. Here $e = 0.99$, $\mu = 1$, and $\beta_0 = 0$.

in Figs. 7(a)–7(d), that follows a complicated nonrepeating pattern. Furthermore, this pattern of collisions in Fig. 8(a) is observed only over the ranges of initial locations x_0 in which the average duration is insensitive to the location in Figs. 7(e)–7(i). When injecting a particle from other locations, the trajectory is widely dispersed throughout the funnel without any clear repeating pattern of collisions. Hence, in these trajectories there is a large probability of the particle falling through the funnel exit after a relatively small number of collisions and in a relatively short time. We have extensively checked other angles and found that the behavior of the average duration versus x_0 is similar to Figs. 7(a)–7(d) for $\theta < 45^\circ$ and similar to Figs. 7(e)–7(i) for $\theta > 45^\circ$. We have also examined the behavior for various values of $-1 < \beta_0 < 1$ and found that they are qualitatively similar to the case when $\beta_0 = 0$ and so we do not present those figures.

IV. THEORETICAL EXPLANATION

In the preceding section we demonstrated numerically that for almost all funnels with angles in the range $\theta > 45^\circ$, the average duration is longer than that in funnels with $\theta < 45^\circ$ when μ and e are sufficiently large. The same surprising phenomenon also occurs for an average impulse and average energy loss. These phenomena are different from those observed in systems with frictionless particles, in which the overall trend is a monotonic function of θ except in the narrow angular ranges in which the anomalous behavior occurs. For frictionless particles, the anomalous behavior occurs only in small ranges of θ , whereas for sufficiently frictional particles the anomalous behavior is highly robust and occurs for all angles $\theta > 45^\circ$. In this section we analyze these phenomena theoretically.

As we showed at the end of Sec. II, when the particle is elastic and the tangential velocity at the contact before the collision is zero, the collision can conserve energy even though there is friction. Therefore, periodic orbits can exist in elastic frictional systems. We now examine the possibility of the existence of periodic orbits and, if so, the stability of the periodic orbits. In contrast to the frictionless case, we will show that, generically, there is a unique type of periodic orbit.

A particle trajectory can be represented by a sequence of collisions. Given a collision sequence, the particle trajectory can be easily determined. Let $Z_i \equiv (u'_i, v'_i, \omega'_i, x_i, y_i)^T$ represent the particle state immediately after the i th collision with the wall, where x_i and y_i are the x and y locations of the i th collision, respectively, u'_i and v'_i are the x and y components of the particle velocity immediately after the i th collision, and ω_i and ω'_i are the angular velocities before and after the i th

collision, respectively. We define C_L and C_R as the operators that determine Z_i from Z_{i-1} if the collision is with the left and right walls, respectively. That is, if the i th collision is with the left wall, we write $Z_i = C_L Z_{i-1}$; if the collision is with the right wall, we write $Z_i = C_R Z_{i-1}$. Hence we can write

$$Z_n = C_n \cdots C_{m+1} Z_m, \quad n > m,$$

where $C_i = C_L$ if the i th collision is with the left wall and $C_i = C_R$ if the i th collision is with the right wall ($i = m + 1, \dots, n$).

Now we show that it is not possible to have $C_{i+1} = C_i$ in an energy-conserving trajectory. That is, it is impossible that both the i th and $(i+1)$ th collisions occur on the same wall. We prove this by the method of contradiction. Without loss of generality, assume that $C_{i+1} = C_i = C_L$. Then, due to energy conservation, the tangential velocity at the contact is zero for general values of β_0 [see Eqs. (7) and (12)] and we have

$$\omega'_i = -\frac{q'_i}{a} = -\frac{u'_i \cos \theta - v'_i \sin \theta}{a}, \quad (13)$$

$$\omega_{i+1} = -\frac{q_{i+1}}{a} = -\frac{u_{i+1} \cos \theta - v_{i+1} \sin \theta}{a}, \quad (14)$$

where q'_i is the tangential velocity of the mass center after the i th collision and q_{i+1} is the tangential velocity of the mass center before the $(i+1)$ th collision. Since there is no torque and no horizontal force during the motion of the particle between the two collisions, we have $\omega_{i+1} = \omega'_i$ and $u_{i+1} = u'_i$. After substituting these expressions into Eqs. (13) and (14), we obtain

$$v_{i+1} = v'_i. \quad (15)$$

In contrast, according to the free-fall motion of the particle between the collisions, we have $v_{i+1} = v'_i - t_i$, where t_i is the time interval between the two collisions. However, $t_i > 0$ and thus $v_{i+1} < v_i$, which contradicts Eq. (15). Similarly, we can show that $C_{i+1} = C_i = C_R$ is impossible. Therefore, any energy-conserving trajectory must have the form $Z_n = \cdots C_L C_R \cdots C_L C_R Z_m$ (assuming that the m th collision is with the left wall), namely, the particle must bounce back and forth between the two walls.

Next we show that there can only be two collisions in a periodic orbit, that is, $Z_m = Z_{m+2} = C_L C_R Z_m$. This is clearly the simplest periodic orbit. Because the tangential velocities at the point of contact are always zero in energy-conserving trajectories [see Eqs. (7) and (12)], we have

$$\omega'_m = -\frac{q'_m}{a} = -\frac{u'_m \cos \theta - v'_m \sin \theta}{a}, \quad (16)$$

$$\omega_{m+1} = -\frac{q_{m+1}}{a} = -\frac{u_{m+1} \cos \theta + v_{m+1} \sin \theta}{a}. \quad (17)$$

The particle experiences gravity only during the free fall between the two collisions, so $\omega'_m = \omega_{m+1}$ and $u'_m = u_{m+1}$. Hence Eqs. (16) and (17) imply that $v_{m+1} = -v'_m$, which implies that $y_{m+1} = y_m$. Similarly, we obtain $y_{m+2} = y_{m+1} = y_m$. Therefore, all collisions occur at the same height on both walls, which we denote by y^* . From the relations $u_{m+1} = u'_m$, $v_{m+1} = -v'_m$, $u_{m+2} = u'_{m+1}$, and $v_{m+2} = -v'_{m+1}$ and the fact that friction has no effect during the collision since the

tangential velocity at the contact point is zero, we obtain the velocity after the $(m+1)$ th and $(m+2)$ th collisions as

$$\begin{aligned} u'_{m+1} &= u'_m \cos 2\theta - v'_m \sin 2\theta, \\ v'_{m+1} &= u'_m \sin 2\theta + v'_m \cos 2\theta, \end{aligned} \quad (18)$$

$$\begin{aligned} u'_{m+2} &= u'_{m+1} \cos 2\theta + v'_{m+1} \sin 2\theta, \\ v'_{m+2} &= -u'_{m+1} \sin 2\theta + v'_{m+1} \cos 2\theta. \end{aligned} \quad (19)$$

Since the collision heights are equal, the time intervals between collisions satisfy

$$t_m = 2v'_m, \quad t_{m+1} = 2v'_{m+1}, \quad t_{m+2} = 2v'_{m+2}, \quad (20)$$

where t_i is the time interval between the i th and $(i+1)$ th collisions. The particle travels over the same horizontal distances in these three time intervals, i.e.,

$$u'_m t_m = -u'_{m+1} t_{m+1} = u'_{m+2} t_{m+2} = 2y^* \cot \theta. \quad (21)$$

From Eqs. (20) and (21) we also have

$$u'_m v'_m = -u'_{m+1} v'_{m+1} = u'_{m+2} v'_{m+2} = y^* \cot \theta. \quad (22)$$

After substituting Eq. (18) into the first equality of Eq. (22) and Eq. (19) into the second equality of Eq. (22), we have

$$\sin 4\theta \left(\frac{v'_m}{u'_m} \right)^2 - 4 \cos^2 2\theta \frac{v'_m}{u'_m} - \sin 4\theta = 0, \quad (23)$$

$$\sin 4\theta \left(\frac{v'_{m+1}}{u'_{m+1}} \right)^2 + 4 \cos^2 2\theta \frac{v'_{m+1}}{u'_{m+1}} - \sin 4\theta = 0. \quad (24)$$

When $\theta \neq 45^\circ$, Eq. (23) gives $v'_m/u'_m = \cot \theta$, which leads to $\omega'_m = -q'_m/a = -(u'_m \cos \theta - v'_m \sin \theta)/a = 0$, and Eq. (24) gives $v'_{m+1}/u'_{m+1} = -\cot \theta$, which leads to $\omega'_{m+1} = -q'_{m+1}/a = -(u'_{m+1} \cos \theta + v'_{m+1} \sin \theta)/a = 0$. After substituting $v'_m/u'_m = \cot \theta$ and $v'_{m+1}/u'_{m+1} = -\cot \theta$ into Eqs. (18) and (19), respectively, we obtain

$$\begin{aligned} u'_{m+1} &= -u'_m, & v'_{m+1} &= v'_m, \\ u'_{m+2} &= -u'_{m+1}, & v'_{m+2} &= v'_{m+1}, \end{aligned}$$

which gives

$$u'_{m+2} = u'_m, \quad v'_{m+2} = v'_m,$$

so $\omega'_{m+2} = -(u'_{m+2} \cos \theta - v'_{m+2} \sin \theta)/a = \omega'_m = 0$. Therefore, we have $Z_{m+2} = Z_m$. So for $\theta \neq 45^\circ$, there is only one type of periodic orbit, which is shown in Fig. 9(a): The velocity of the center of mass is perpendicular to the wall and the tangential velocity at contact is zero. This implies that particles executing this type of periodic orbit do not rotate for funnel angles $\theta \neq 45^\circ$.

When $\theta = 45^\circ$, $\sin 4\theta = \cos 2\theta = 0$, so Eqs. (23) and (24) are automatically satisfied, and from Eqs. (18) and (19) we obtain $u'_{m+1} = -v'_m$, $v'_{m+1} = u'_m$, $u'_{m+2} = v'_{m+1}$, and $v'_{m+2} = -u'_{m+1}$. So $u'_{m+2} = u'_m$, $v'_{m+2} = v'_m$, and therefore we have also $Z_{m+2} = Z_m$. For this case the periodic orbit is shown in Fig. 9(b). We note that in this case the rotation of the particle can occur.

Therefore, as one drops a frictional elastic particle into a funnel with no exit, only two possible final states can exist: (i) The particle loses all its energy and rests on the bottom of the

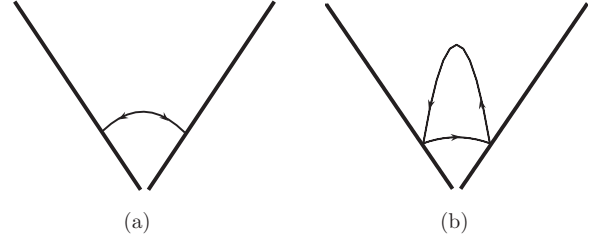


FIG. 9. Periodic orbits for $e = 1$ with (a) $\theta \neq 45^\circ$ and (b) $\theta = 45^\circ$.

funnel or (ii) the particle evolves into a simplest orbit of period 2, in which the particle bounces back and forth between the two walls with both collisions occurring at the same height.

The above theoretical analysis shows the possibility of the existence of periodic orbits. However, for such periodic orbits to be realizable, the orbits must also be stable. Otherwise, any infinitesimal deviation will eventually drive the particle away from the periodic orbit. Since no funnel can be perfectly 45° , we need to consider only the orbit shown in Fig. 9(a), which exists in funnels with $\theta \neq 45^\circ$.

To determine the states in the periodic orbits and the stability of these orbits, we need to construct a map of the collisions in an orbit that follows the sequence C_L first and then C_R . Since x_i and y_i are constrained to be on the funnel boundaries, we can eliminate x_i in favor of y_i . We need to consider only $i = 1, 2, 3$ since the orbit under consideration is period 2. Furthermore, we need to consider only the case in which Eqs. (10) and (11) apply because we consider the perturbation of the periodic orbit in which the tangential velocity of the contact point before collision is infinitesimally small, so any small friction can reduce it to zero before the collision ends. We comment that these two equations also hold for the situation in which the particle loses all its energy, namely, $q' = q = \omega' = \omega = 0$. The orbit is completely specified by $\mathbf{P}_i = (y_i, u'_i, v'_i, \omega'_i)^T$ for $i = 1, 2, 3$. Given \mathbf{P}_1 , we can determine \mathbf{P}_2 by constructing the map \mathbf{F}_1 defined by $\mathbf{P}_2 = \mathbf{F}_1(\mathbf{P}_1)$ as follows. The first and second collisions are on the left and right walls, respectively, so we have

$$y_1 = -x_1 \tan \theta, \quad y_2 = x_2 \tan \theta. \quad (25)$$

Between collisions the center of mass of the particle experiences free-fall motion under gravity and we have

$$y_2 = y_1 + v'_1 t_1 - \frac{1}{2} g t_1^2, \quad x_2 = x_1 + u'_1 t_1. \quad (26)$$

This allows us to determine t , the time interval between the two collisions, by eliminating x_1 , x_2 , and y_2 from the above expressions; the result is

$$t_1 = v'_1 - u'_1 \tan \theta + \sqrt{(v'_1 - u'_1 \tan \theta)^2 + 4y_1}. \quad (27)$$

Then the location and the x and y components of the velocity immediately before the second collision can be obtained from Eqs. (25)–(27):

$$\begin{aligned} y_2 &= x_2 \tan \theta = (x_1 + u'_1 t_1) \tan \theta = -y_1 + u'_1 t_1 \tan \theta, \\ u_2 &= u'_1, \end{aligned} \quad (28)$$

$$v_2 = v'_1 - t_1 = u'_1 \tan \theta - \sqrt{(v'_1 - u'_1 \tan \theta)^2 + 4y_1}.$$

The velocity of the center of mass perpendicular to the wall immediately before the second collision can be expressed in terms of u_2 and v_2 ,

$$p_2 = -u_2 \sin \theta + v_2 \cos \theta = -\cos \theta \sqrt{(v'_1 - u'_1 \tan \theta)^2 + 4y_1},$$

Therefore, after the second collision, this velocity component becomes

$$p'_2 = -p_2 = \cos \theta \sqrt{(v'_1 - u'_1 \tan \theta)^2 + 4y_1}. \quad (29)$$

The velocity of the center of mass tangential to the wall immediately before the second collision is

$$q_2 = u_2 \cos \theta + v_2 \sin \theta = u'_1 \sec \theta - \sin \theta \sqrt{(v'_1 - u'_1 \tan \theta)^2 + 4y_1}$$

and the angular velocity is

$$\omega_2 = \omega'_1.$$

According to Eq. (10) we have

$$\begin{aligned} q'_2 &= \frac{ma^2 - I\beta_0}{I + ma^2} q_2 - \frac{Ia}{I + ma^2} (1 + \beta_0) \omega_2 \\ &= \frac{ma^2 - I\beta_0}{I + ma^2} [u'_1 \sec \theta - \sin \theta \sqrt{(v'_1 - u'_1 \tan \theta)^2 + 4y_1}] \\ &\quad - \frac{Ia}{I + ma^2} (1 + \beta_0) \omega'_1. \end{aligned} \quad (30)$$

The x and y components of the velocity immediately after the second collision can easily be determined from Eqs. (29) and (30) to give

$$\begin{aligned} u'_2 &= q'_2 \cos \theta - p'_2 \sin \theta = \frac{ma^2 - I\beta_0}{I + ma^2} u'_1 \\ &\quad - \frac{Ia}{I + ma^2} (1 + \beta_0) \cos \theta \omega'_1 - \frac{2ma^2 + I(1 - \beta_0)}{I + ma^2} \\ &\quad \times \sin \theta \cos \theta \sqrt{(v'_1 - u'_1 \tan \theta)^2 + 4y_1}, \end{aligned} \quad (31)$$

$$\begin{aligned} v'_2 &= q'_2 \sin \theta + p'_2 \cos \theta \\ &= \frac{ma^2 - I\beta_0}{I + ma^2} \tan \theta u'_1 - \frac{Ia}{I + ma^2} (1 + \beta_0) \sin \theta \omega'_1 \\ &\quad + \left(1 - \frac{2ma^2 + I(1 - \beta_0)}{I + ma^2} \sin^2 \theta\right) \\ &\quad \times \sqrt{(v'_1 - u'_1 \tan \theta)^2 + 4y_1}. \end{aligned} \quad (32)$$

The angular velocity immediately after the second collision is given by Eq. (11),

$$\begin{aligned} \omega'_2 &= -\frac{ma(1 + \beta_0)}{I + ma^2} q_2 + \frac{I - ma^2 \beta_0}{I + ma^2} \omega_2 \\ &= -\frac{ma(1 + \beta_0)}{I + ma^2} [u'_1 \sec \theta - \sin \theta \sqrt{(v'_1 - u'_1 \tan \theta)^2 + 4y_1}] \\ &\quad + \frac{I - ma^2 \beta_0}{I + ma^2} \omega'_1. \end{aligned} \quad (33)$$

Thus Eqs. (28) and (31)–(33) can be combined to give the map $\mathbf{P}_2 = \mathbf{F}_1(\mathbf{P}_1)$, which determines the location and velocities

immediately after the second collision in terms of the location and velocities immediately after the first collision. Following similar steps, we can derive the map from the second collision to the third collision $\mathbf{P}_3 = \mathbf{F}_2(\mathbf{P}_2)$:

$$y_3 = -y_2 - u'_2 \tan \theta t_2, \quad (34)$$

$$\begin{aligned} u'_3 &= \frac{ma^2 - I\beta_0}{I + ma^2} u'_2 - \frac{Ia(1 + \beta_0)}{I + ma^2} \cos \theta \omega'_2 \\ &\quad + \frac{2ma^2 + I(1 - \beta_0)}{I + ma^2} \\ &\quad \times \sin \theta \cos \theta \sqrt{(v'_2 + u'_2 \tan \theta)^2 + 4y_2}, \end{aligned} \quad (35)$$

$$\begin{aligned} v'_3 &= -\frac{ma^2 - I\beta_0}{I + ma^2} \tan \theta u'_2 + \frac{Ia(1 + \beta_0)}{I + ma^2} \sin \theta \omega'_2 \\ &\quad + \left(1 - \frac{2ma^2 + I(1 - \beta_0)}{I + ma^2} \sin^2 \theta\right) \\ &\quad \times \sqrt{(v'_2 + u'_2 \tan \theta)^2 + 4y_2}, \end{aligned} \quad (36)$$

$$\begin{aligned} \omega'_3 &= -\frac{ma(1 + \beta_0)}{I + ma^2} [u'_2 \sec \theta + \sin \theta \sqrt{(v'_2 + u'_2 \tan \theta)^2 + 4y_2}] \\ &\quad + \frac{I - ma^2 \beta_0}{I + ma^2} \omega'_2, \end{aligned} \quad (37)$$

where $t_2 = v'_2 + u'_2 \tan \theta + \sqrt{(v'_2 + u'_2 \tan \theta)^2 + 4y_2}$ is the time interval from the second collision to the third. By combining the two maps we obtain a map from the first collision to the third $\mathbf{P}_3 = \mathbf{F}(\mathbf{P}_1)$.

Since the motion is periodic, we know that $\mathbf{P}_1 = \mathbf{P}_3 = \mathbf{F}(\mathbf{P}_1)$. The solution of this set of nonlinear equations determines the existence of the periodic orbit shown in Figs. 9(a) and 9(b). Let \mathbf{P}_1^* be the solution to the equation $\mathbf{P}_1^* = \mathbf{F}(\mathbf{P}_1^*)$. One can easily show that a solution always exists for all values of θ . From $u_1^* v_1^* = y^* \cot \theta$ and $v_1^*/u_1^* = \cot \theta$ given by Eqs. (22) and (23), we obtain $u_1^* = \sqrt{y^*}$, $v_1^* = \sqrt{y^*} \cot \theta$, $u_2^* = -\sqrt{y^*}$, $v_2^* = \sqrt{y^*} \cot \theta$, and $\omega_1^* = \omega_2^* = 0$. However, the equilibrium height of the periodic orbit y^* cannot be determined using the above arguments. When the particle is initially released, it must experience frictional losses until it eventually reaches the periodic orbit. The amount of energy loss determines the height. Different initial locations follow different trajectories as they evolve toward a periodic orbit and so they lose different amounts of energy.

To determine the stability, we perturb \mathbf{P}_1 by $d\mathbf{P}_1$ and then \mathbf{P}_2 and \mathbf{P}_3 will change by $d\mathbf{P}_2$ and $d\mathbf{P}_3$, respectively. We can use the map \mathbf{F} derived above in our stability analysis. Since $\mathbf{P}_2 = \mathbf{F}_1(\mathbf{P}_1)$ and $\mathbf{P}_3 = \mathbf{F}_2(\mathbf{P}_2) = \mathbf{F}_2[\mathbf{F}_1(\mathbf{P}_1)]$, application of the chain rule gives

$$d\mathbf{P}_3 = \left. \frac{d\mathbf{F}}{d\mathbf{P}_1} \right|_{\mathbf{P}_1=\mathbf{P}_1^*}, \quad d\mathbf{P}_1 = \left. \frac{d\mathbf{F}_2}{d\mathbf{P}_2} \right|_{\mathbf{P}_2=\mathbf{P}_2^*} \cdot \left. \frac{d\mathbf{F}_1}{d\mathbf{P}_1} \right|_{\mathbf{P}_1=\mathbf{P}_1^*} d\mathbf{P}_1. \quad (38)$$

Using the maps given by Eqs. (28) and (31)–(36), we obtain

$$\frac{d\mathbf{F}_1}{d\mathbf{P}_1} \Big|_{\mathbf{P}_1=\mathbf{P}_1^*} = \frac{\partial(y_2, u'_2, v'_2, \omega'_2)}{\partial(y_1, u'_1, v'_1, \omega'_1)} \Big|_{\mathbf{P}_1=\mathbf{P}_1^*} = \begin{pmatrix} -\cos 2\theta & 2\sqrt{y^*} \cos^2 \theta & \sqrt{y^*} \sin 2\theta & 0 \\ -\frac{1}{2\sqrt{y^*}}(1+c) \sin^2 2\theta & (1+c) \sin^2 \theta \cos 2\theta + c & -\frac{1}{4}(1+c) \sin 4\theta & -a(1-c) \cos \theta \\ \frac{1}{\sqrt{y^*}}(\cos^2 \theta - c \sin^2 \theta) \sin 2\theta & -(\cos^2 \theta - c \sin^2 \theta) \tan \theta \cos 2\theta + c \tan \theta & (\cos^2 \theta - c \sin^2 \theta) \cos 2\theta & -a(1-c) \sin \theta \\ \frac{ma}{I\sqrt{y^*}}(1-c) \sin 2\theta \sin \theta & -\frac{ma}{I}(1-c) \sec \theta (1 + \cos 2\theta \sin^2 \theta) & \frac{ma}{I}(1-c) \sin \theta \cos 2\theta & 1 - c - \beta_0 \end{pmatrix}$$

and

$$\frac{d\mathbf{F}_2}{d\mathbf{P}_2} \Big|_{\mathbf{P}_2=\mathbf{P}_2^*} = \frac{\partial(y_3, u'_3, v'_3, \omega'_3)}{\partial(y_2, u'_2, v'_2, \omega'_2)} \Big|_{\mathbf{P}_2=\mathbf{P}_2^*} = \begin{pmatrix} -\cos 2\theta & -2\sqrt{y^*} \cos^2 \theta & \sqrt{y^*} \sin 2\theta & 0 \\ \frac{1}{2\sqrt{y^*}}(1+c) \sin^2 2\theta & (1+c) \sin^2 \theta \cos 2\theta + c & \frac{1}{4}(1+c) \sin 4\theta & -a(1-c) \cos \theta \\ \frac{1}{\sqrt{y^*}}(\cos^2 \theta - c \sin^2 \theta) \sin 2\theta & (\cos^2 \theta - c \sin^2 \theta) \tan \theta \cos 2\theta - c \tan \theta & (\cos^2 \theta - c \sin^2 \theta) \cos 2\theta & a(1-c) \sin \theta \\ -\frac{ma}{I\sqrt{y^*}}(1-c) \sin 2\theta \sin \theta & -\frac{ma}{I}(1-c) \sec \theta (1 + \cos 2\theta \sin^2 \theta) & -\frac{ma}{I}(1-c) \sin \theta \cos 2\theta & 1 - c - \beta_0 \end{pmatrix},$$

where $c \equiv \frac{ma^2 - I\beta_0}{I + ma^2}$. The stability of the orbit can be found by considering the eigenvalues of the matrix $\frac{d\mathbf{F}_2}{d\mathbf{P}_2} \Big|_{\mathbf{P}_2=\mathbf{P}_2^*} \frac{d\mathbf{F}_1}{d\mathbf{P}_1} \Big|_{\mathbf{P}_1=\mathbf{P}_1^*}$. Although the elements of the matrix $\frac{d\mathbf{F}_2}{d\mathbf{P}_2} \Big|_{\mathbf{P}_2=\mathbf{P}_2^*} \frac{d\mathbf{F}_1}{d\mathbf{P}_1} \Big|_{\mathbf{P}_1=\mathbf{P}_1^*}$ depend on y^* , the characteristic polynomial for the eigenvalues of this matrix does not. Therefore, the stability condition of the orbit also will not depend on y^* . One can readily show that one of the eigenvalues λ_4 is always 1. Therefore, if $|\lambda_i| < 1$ ($i = 1, 2, 3$), the orbit is linearly stable, which means that trajectories that start sufficiently close to the periodic orbit will approach the periodic orbit. When $|\lambda_1| > 1$, $|\lambda_2| > 1$, or $|\lambda_3| > 1$, trajectories that start close to the periodic orbit

will diverge from the periodic orbit until the particle can no longer follow the collision sequence. In Fig. 10 we plot the magnitudes of the eigenvalues as a function of funnel angle for $\beta_0 = 0.31$ when the particle is a sphere, i.e., $I = \frac{2}{5}ma^2$. Figure 10 illustrates that the orbit given by Fig. 9(a) is always unstable for $\theta < 45^\circ$ and is always stable for $\theta > 45^\circ$. When $\beta_0 = 0$, the conditions for stability can be calculated analytically and we can prove that the range of θ for stability is larger than 45° (see the Appendix). For other values of $\beta_0 \in (-1, 1)$, one can show that $\lambda_1 = \lambda_2 = 1$ at $\theta = 45^\circ$, which suggests that there is a change of stability at $\theta = 45^\circ$; extensive numerical tests indicate that the orbit is stable for $\theta > 45^\circ$ and unstable for $\theta < 45^\circ$.

For $\theta > 45^\circ$, even in the case of small friction, a particle can approach the periodic state. However, one cannot determine the height y^* of the periodic state explicitly. This is because the height y^* is determined by the energy loss during the initial part of the trajectory; this represents a complicated nonlinear dynamical problem. Although the analytical process is difficult, it is straightforward to study this problem numerically. To study the dependence of the periodic state on the initial location of the particle x_0 we perform simulations for an elastic frictional particle in a closed funnel ($d = 0$) and record the x locations of the periodic state for a given initial location x_0 . In Fig. 11 we plot the result for $\theta = 50^\circ$, $\beta_0 = 0$, and several different values of μ . There are only two final states: a periodic state, in which the particle follows the periodic motion analyzed above, or a dead state, in which the particle loses all of its energy and rests at the bottom of the funnel. The dead state is represented by a single point located on the axis $y = 0$ and a periodic orbit is represented by two points located symmetrically about the axis $y = 0$. We comment that in Fig. 11, at certain initial locations, the vertical points appear to be widely spread [especially in Fig. 11(a)]. One may think that this corresponds to orbits with period longer than 2, which contradicts the orbit shown in Fig. 9(a). Since this is not the case, there are only two collision points for each given initial location. Thus Fig. 9(a) is indeed

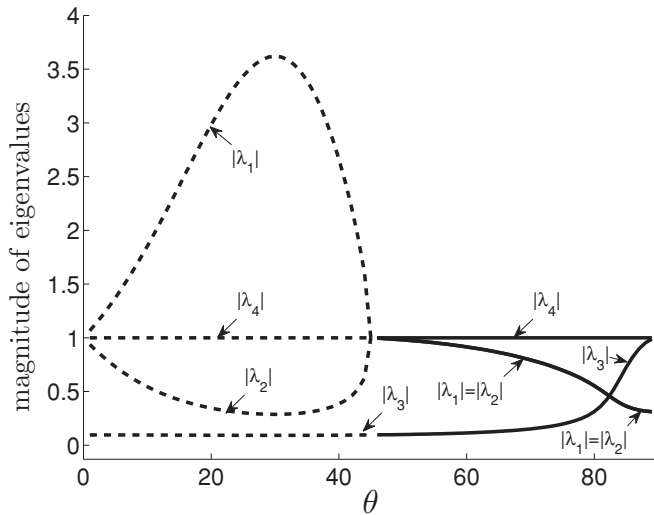


FIG. 10. Stability of the orbit shown in Fig. 9(a) for $\beta_0 = 0.31$. The magnitude of the eigenvalues of $\frac{\partial\mathbf{F}(\mathbf{P}_1)}{\partial\mathbf{P}_1}$ is shown as a function of θ when the moment of inertia $I = \frac{2}{5}ma^2$. The solid curves indicate the range of θ for which the corresponding orbit is neutrally linearly stable. The dashed curves indicate the range of θ for which the corresponding orbit is neutrally unstable.

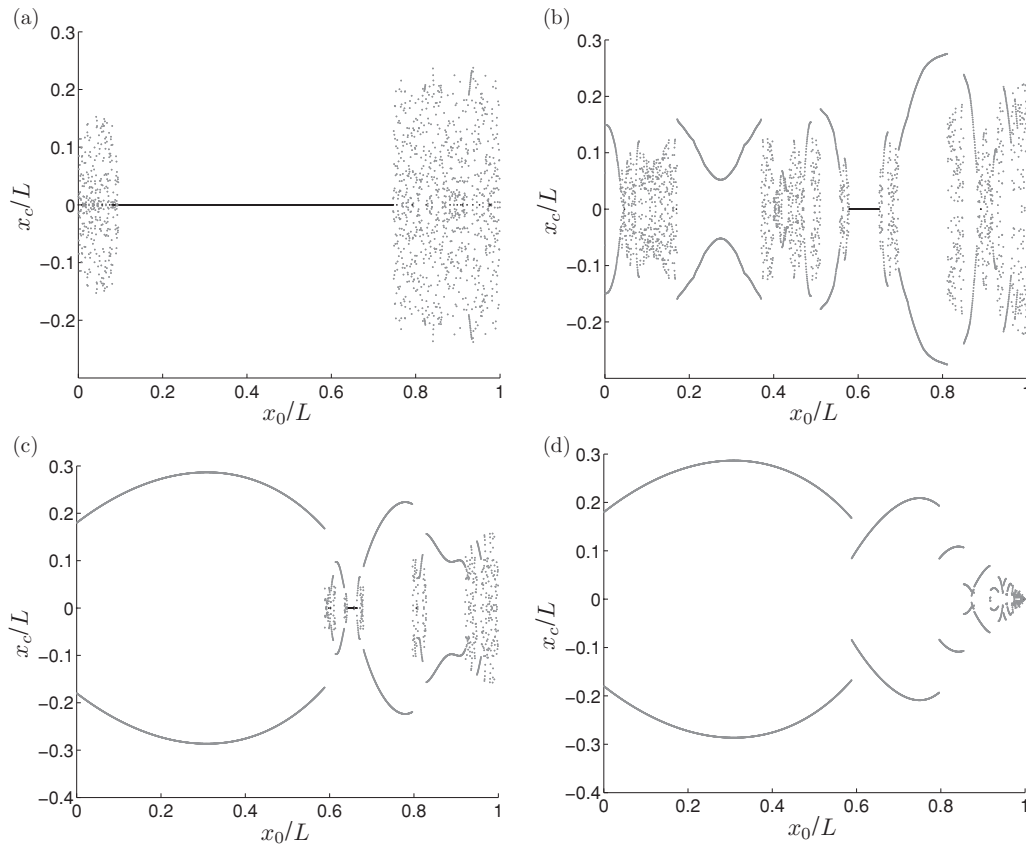


FIG. 11. Scaled x locations of the collisions (x_c/L) after the particle has reached a periodic orbit plotted as a function of the scaled input locations (x_0/L) for $\theta = 50^\circ$, $e = 1$, $\beta_0 = 0$, and different values of μ : (a) $\mu = 0.01$, (b) $\mu = 0.1$, (c) $\mu = 0.2$, and (d) $\mu = 1$. The funnel is closed, i.e., $d = 0$. The collision locations for the particles that eventually reach a periodic orbit are shown in gray. For any value of x_0/L , there are only two points that are symmetric with respect to the origin. The dark points represent collision locations for the other particles, which do not reach periodic orbits and eventually lose all of their energy. The x locations of these points are all zero. Here L is half the effective opening of the funnel for the center of the particle (see Fig. 1).

the only stable periodic orbit. The spread of the points is due to the high sensitivity of trajectories (and hence energy loss) on the initial location. Figure 11(a) is for systems with small μ ; therefore, it takes more collisions to damp out the tangential velocity at the contact point and, consequently, longer to reach the periodic orbit. Therefore, it will be more sensitive to the initial location. As μ increases, fewer collisions are needed to reach the condition $\mu > \mu_c$; therefore, the location of the collision point at the final periodic state will become less sensitive to the initial location. Figure 11 indeed shows this. Since the particle is dropped into the funnel randomly with each initial location having a uniform probability, it is natural to ask what the probability is of reaching a periodic orbit as its final state. This probability is plotted in Fig. 12 as a function of μ for different values of θ . Figure 12 shows that for $\theta > 60^\circ$, the probability quickly reaches 100% at very small values of μ . We have shown theoretically that the probability is zero when $\theta < 45^\circ$. We also performed simulations for other angles in the range $\theta > 45^\circ$; the results are similar to Fig. 11 for $\theta = 50^\circ$. The general trend is the following: For given μ , the larger θ is, the higher the probability that the system reaches the periodic orbit shown in Fig. 9(a). Investigations for other values of β_0 reveal behavior similar to that shown in Figs. 11 and 12.

The above analysis allows us to explain the surprising results shown in Figs. 3–5. This is due to the key fact that the stable periodic orbit always exists in funnels with $\theta > 45^\circ$ and

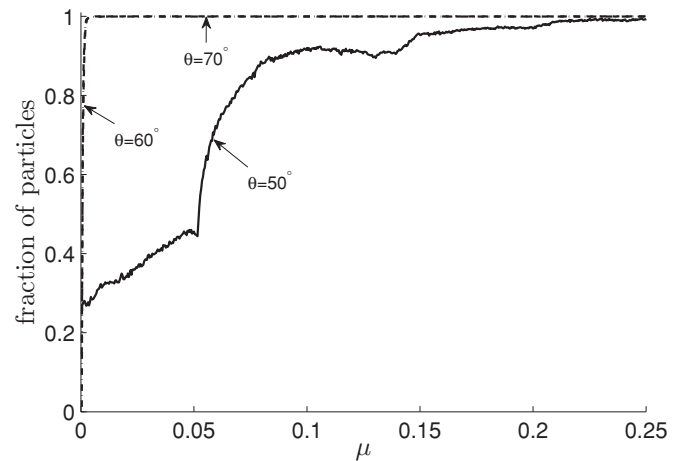


FIG. 12. Fraction of particles that can reach the periodic orbit plotted as a function of μ for $e = 1$, $\beta_0 = 0$, and different values of θ (50° , 60° , and 70°). The curve with $\theta = 60^\circ$ and that with $\theta = 70^\circ$ almost coincide.

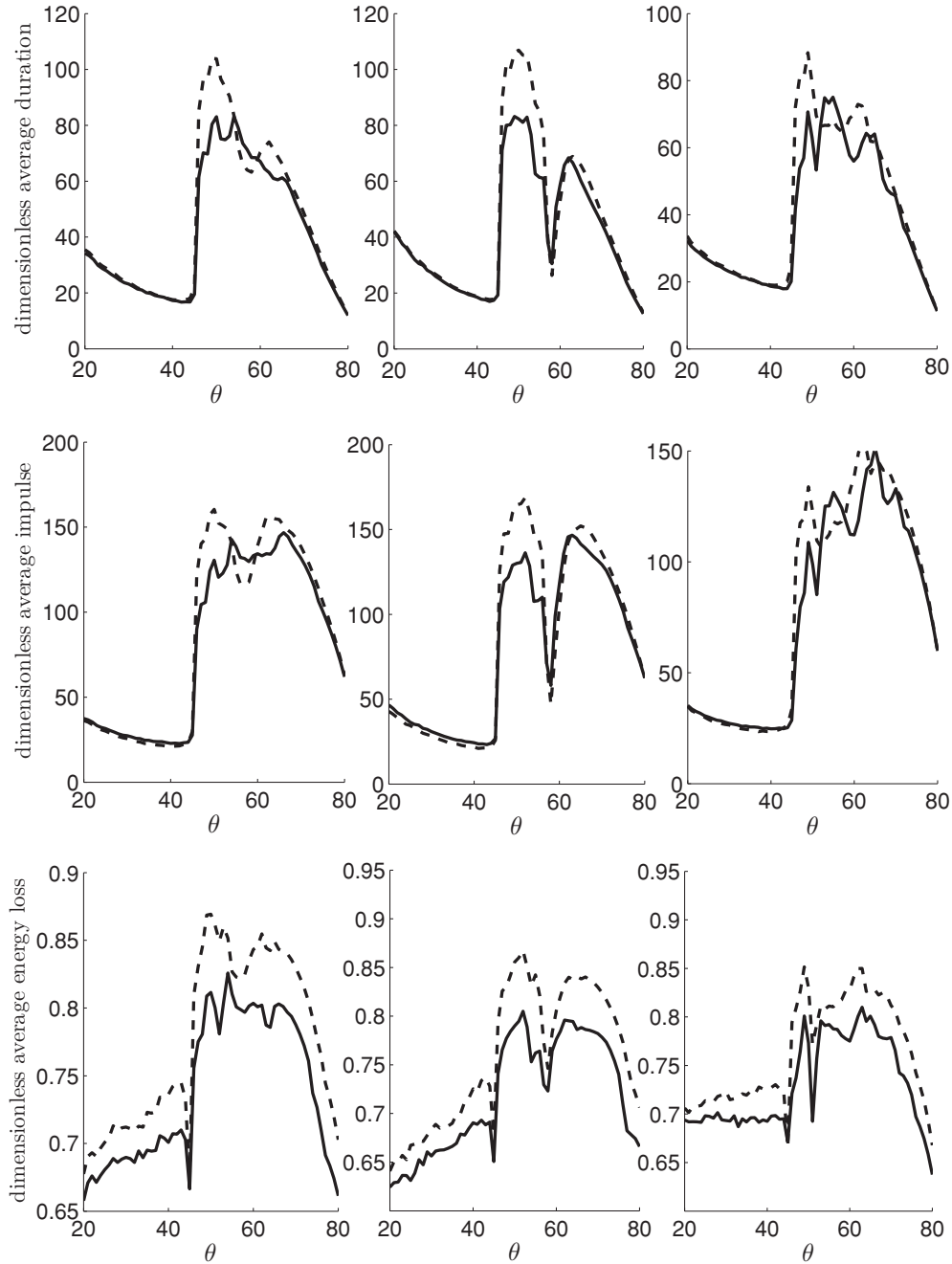


FIG. 13. Average duration (nondimensionalized by $\sqrt{H/g}$), impulse (nondimensionalized by $m\sqrt{gH}$), and energy loss (nondimensionalized by mgH) plotted against θ for axisymmetric conical funnels (solid curves) and two-dimensional funnels (dashed curves) with $\mu = 1$ and $e = 0.99$, respectively. From left to right, the plots correspond to $\beta_0 = 0, 0.31,$ and -0.31 , respectively.

cannot exist in funnels with $\theta < 45^\circ$. In general, when $e < 1$, no periodic orbit can exist due to energy loss during collisions. However, when e is close to 1, particle trajectories in funnels with $\theta > 45^\circ$ can follow the same pattern of hopping between left and right walls. The main difference between the orbit for $e = 1$ and that for e close to 1 is that, for $e = 1$, the collision location y will remain the same, while for $e \approx 1$, y will slowly decrease. The situation for $\theta < 45^\circ$ is very different. No orbit can exist for $e = 1$; therefore, for $e \approx 1$, the collision points will be widely scattered within the funnel. This leads to a large probability that the particle hits the exit in a relatively small

number of collisions. This is why the average duration that the particle stays inside a funnel with $\theta > 45^\circ$ is larger than that in funnels with $\theta < 45^\circ$. The phenomena demonstrated in Figs. 4 and 5 can be explained in a similar way by considering the existence of the periodic orbits shown in Fig. 9(a).

V. AXISYMMETRIC CONICAL FUNNEL

We have also examined the case of an axisymmetric conical funnel, i.e., a single frictional, inelastic ball with zero initial velocity and zero initial angular velocity falling under gravity

through a funnel of conical shape. In this case, the center of the particle always remains in the same plane and so the dynamics is identical to the case above. The only difference is in the distribution of the initial locations, which we assume to be uniformly distributed over the circle at the top of the funnel rather than uniformly distributed over the line in the two-dimensional case. In Fig. 13 we plot the average duration, average impulse, and average energy loss with $e = 0.99$, $\mu = 1$, and three different values of β_0 (from left to right the plots correspond to $\beta_0 = 0, 0.31$, and -0.31 , respectively). For convenience of comparison, the results from two-dimensional funnels with the same parameters are also shown in Fig. 13 as dashed curves. Figure 13 clearly show that the anomalous behavior still exists for the conical funnel with $\mu = 1$ and is very similar to that shown in funnels in two dimensions. The behavior for $\theta > 45^\circ$ is very different from that for $\theta < 45^\circ$ in axisymmetric conical funnels as well. We comment that since the trajectory of a particle in an axisymmetric conical funnel is identical to that in a two-dimensional funnel, if both particles have zero velocity and zero angular velocity and have the same initial distance from the symmetry axis, our construction and stability analysis for the periodic orbit in the two-dimensional funnels remain valid for the axisymmetric conical funnel. It follows that the anomalous phenomenon shown in Fig. 13 is also due to the existence of the same simplest quasiperiodic orbit.

VI. CONCLUSION

We have studied systems in which a frictional, inelastic particle falls through a symmetric funnel with flat walls inclined at an angle θ to the horizontal (see Fig. 1). Our study has shown that the anomalous phenomena that we found in a similar system with a frictionless particle not only exist, but are also dramatically enhanced in systems with a frictional particle (see Figs. 3–5). The main features of the anomalous phenomena are that a particle may stay longer, exert bigger impulses to the walls, and lose more energy in a steeper funnel than that in a less steep funnel. The anomalous phenomena in frictional particle systems may appear to be similar to the anomalous phenomena observed in the frictionless particle systems, namely, the anomalous phenomena exist only in funnels with $\theta > 45^\circ$ and they are the consequences of the existence of stable quasiperiodic orbits (i.e., repeated patterns in the particle-wall collision sequences). However, the behavior of frictional particles is very different from that of frictionless particles. For frictionless particles ($\mu = 0$), there are only certain narrow ranges of θ in which the anomalous behavior occurs (see the peaks of the curve for $\mu = 0$ in Fig. 3). It has been shown in Ref. [1] that these peaks correspond to an infinite set of periodic orbits, some examples of which are shown in Fig. 14. In this paper we have proved that all these orbits cannot exist even for infinitesimally small μ and they all evolve into a new stable orbit given by Fig. 9(a). We emphasize that this new orbit cannot be realized by dropping a frictionless, elastic particle into a funnel. This is due to the fact that the trajectories of a frictionless elastic particle are time reversible. This means that, for a periodic orbit, the particle must return to its initial dropping point. At this point, the particle must have zero velocity due to

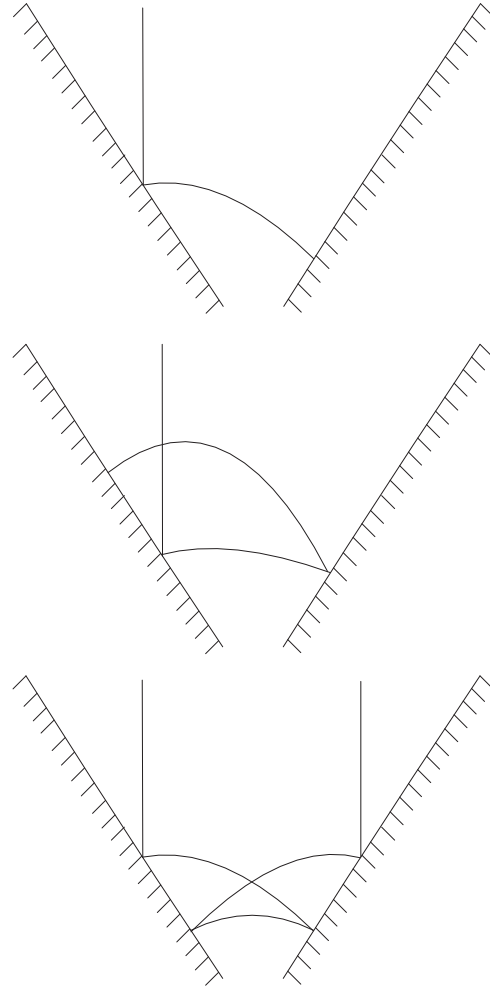


FIG. 14. Three simplest orbits in an elastic frictionless system determined in Ref. [1].

energy conservation. This is clearly incompatible with the new orbit in Fig. 9(a), whose velocity is always nonzero. We also emphasize that this new stable orbit always exist for any funnel with $\theta > 45^\circ$ in frictional particle systems. Therefore, friction plays a critical role in determining the dynamics of a particle falling through a funnel. We have also shown that the same anomalous phenomena also exist when a frictional, inelastic particle falls through an axisymmetric conical funnel due to the same physical mechanism.

ACKNOWLEDGMENT

This work was fully supported by the Research Grants Council of Hong Kong Special Administrative Region, China, Project No. CityU 102909.

APPENDIX: PROOF OF THE STABLE RANGE OF θ WHEN $\beta_0 = 0$

For $\beta_0 = 0$, one can readily show that the eigenvalues of $\frac{d\mathbf{F}}{d\mathbf{P}_1}|_{\mathbf{P}_1=\mathbf{P}_1^*} = \frac{d\mathbf{F}_2}{d\mathbf{P}_2}|_{\mathbf{P}_2=\mathbf{P}_2^*} \frac{d\mathbf{F}_1}{d\mathbf{P}_1}|_{\mathbf{P}_1=\mathbf{P}_1^*}$ are given by

$$\begin{aligned} \lambda_1 &= A + \sqrt{A^2 + B}, & \lambda_2 &= A - \sqrt{A^2 + B}, \\ \lambda_3 &= 0, & \lambda_4 &= 1, \end{aligned} \quad (\text{A1})$$

where

$$A \equiv 8(1+c)^2\eta^4 - 8(1+c)^2\eta^3 - 2(1-c^2+4c)\eta^2 + 2(1+3c)\eta + 1, \quad (\text{A2})$$

$$B \equiv -16(1-c)^2\eta^4 + 16(1-c)^2\eta^3 + 4(1-c^2)\eta^2 - 4(1-c)\eta - 1, \quad (\text{A3})$$

and $\eta = \sin^2\theta$. We can prove that $|\lambda_1| < 1$ and $|\lambda_2| < 1$ if and only if $\theta < 45^\circ$. The eigenvalues λ_1 and λ_2 can be either complex or real; we consider these two cases separately.

We begin by considering the case in which λ_1 and λ_2 are complex. From Eq. (A1), λ_1 and λ_2 will be complex if $B < -A^2$. In this case, the norms of λ_1 and λ_2 are given by Eqs. (A1),

$$|\lambda_1| = |A + \sqrt{A^2 + B}| = |A + i\sqrt{-A^2 - B}| = -B,$$

$$|\lambda_2| = |A - \sqrt{A^2 + B}| = |A - i\sqrt{-A^2 - B}| = -B.$$

Hence $|\lambda_1| < 1$ and $|\lambda_2| < 1$ can hold only if $B > -1$. So we need to compute the range of θ such that $B > -1$. From Eq. (A3) we obtain

$$B + 1 = -16(1-c)^2\eta^4 + 16(1-c)^2\eta^3 + 4(1-c^2)\eta^2 - 4(1-c)\eta. \quad (\text{A4})$$

The roots of $B + 1 = 0$ are given by $\eta_1 = 0$, $\eta_2 = \frac{1}{2}$, $\eta_3 = \frac{1}{4} + \frac{1}{4}\sqrt{1 + \frac{8}{1-c}}$, and $\eta_4 = \frac{1}{4} - \frac{1}{4}\sqrt{1 + \frac{8}{1-c}}$. Using the fact that $c = \frac{ma^2}{I+ma^2} \in (0,1)$, one can readily show that $\eta_3 > 1$ and $\eta_4 < 0$. Since $\eta = \sin^2\theta$, the only physically relevant root is $\eta = \frac{1}{2}$, which corresponds to $\theta = 45^\circ$. One can further show that $|\lambda_1| < 1$ and $|\lambda_2| < 1$ if $\theta > 45^\circ$ and $B < -A^2$.

We now consider the case in which $|\lambda_1|$ and $|\lambda_2|$ are real. From Eq. (A1), $|\lambda_1|$ and $|\lambda_2|$ will be real if $B \geq -A^2$. Using Eq. (A1), $|\lambda_1| < 1$ and $|\lambda_2| < 1$ will be true if and only if

$$-1 - A < \sqrt{A^2 + B} < 1 - A, \quad (\text{A5})$$

$$-1 + A < \sqrt{A^2 + B} < 1 + A, \quad (\text{A6})$$

which can be written as

$$A > -1, \quad B - 2A < 1, \quad A < 1, \quad B + 2A < 1. \quad (\text{A7})$$

Now we prove that A is always larger than -1 . From Eq. (A2) we obtain

$$A + 1 = 8(1+c)^2\eta^4 - 8(1+c)^2\eta^3 - 2(1-c^2+4c)\eta^2 + 2(1+3c)\eta + 2. \quad (\text{A8})$$

To prove that the quantity $A + 1$ is always larger than zero, one must determine its stationary values and its values at the boundary points (0 and 1). The stationary values of $A + 1$ can be found by solving

$$32(1+c)^2\eta^3 - 24(1+c)^2\eta^2 - 4(1-c^2+4c)\eta + 2(1+3c) = 0,$$

which yields $\eta = \frac{1}{4}$ and $\frac{1}{4} \pm \frac{1}{4}\sqrt{1 + \frac{4(1+3c)}{(1+c)^2}}$. Among these roots $\frac{1}{4} - \frac{1}{4}\sqrt{1 + \frac{4(1+3c)}{(1+c)^2}} < 0$, so by evaluating $A + 1$ at the boundary values $\eta = 0, 1$ and the stationary points $\eta = \frac{1}{4}, \frac{1}{4} + \frac{1}{4}\sqrt{1 + \frac{4(1+3c)}{(1+c)^2}}$ in Eq. (A8), it is easy to see that $A + 1 > 0$ for all $\eta \in [0, 1]$ and $c = \frac{ma^2}{I+ma^2} \in (0, 1)$.

Next we prove that $B - 2A$ is always smaller than 1. From the expressions of A and B we get

$$B - 2A - 1 = -32(1+c^2)\eta^4 + 32(1+c^2)\eta^3 + 8(1-c^2+2c)\eta^2 - 8(1+c)\eta - 4. \quad (\text{A9})$$

The stationary points of this quantity are given by solving

$$-128(1+c)^2\eta^3 + 96(1+c)^2\eta^2 + 16(1-c^2+4c)\eta - 8(1+c) = 0,$$

which yields $\eta = \frac{1}{4}$ and $\frac{1}{4} \pm \frac{1}{4}\sqrt{1 + \frac{4(1+c)}{1+c^2}}$. It is then straightforward to show that $B - 2A < 1$ for all $\eta \in [0, 1]$ and $c \in (0, 1)$.

Next we compute the range of θ for which $A < 1$. From Eq. (A2) we have

$$A - 1 = 8(1+c)^2\eta^4 - 8(1+c)^2\eta^3 - 2(1-c^2+4c)\eta^2 + 2(1+3c)\eta, \quad (\text{A10})$$

which has zeros at $\eta_1 = 0$, $\eta_2 = \frac{1}{2}$, $\eta_3 = \frac{1}{4} + \frac{1}{4}\sqrt{1 + \frac{8(1+3c)}{(1+c)^2}}$, and $\eta_4 = \frac{1}{4} - \frac{1}{4}\sqrt{1 + \frac{8(1+3c)}{(1+c)^2}}$. It is easy to see that $\eta_3 > 1$ and $\eta_4 < 0$ and that $A - 1 < 0$ if and only if $\eta > \frac{1}{2}$, that is, $\theta > 45^\circ$. Finally, we compute the range of θ for which $B + 2A < 1$. From Eqs. (A1) and (A2) we have

$$B + 2A - 1 = 64c\eta^4 - 64c\eta^3 - 16c\eta^2 + 16c\eta, \quad (\text{A11})$$

which has zeros at $\eta = -\frac{1}{2}, 0, \frac{1}{2}$, and 1, and it is easy to show that $B + 2A - 1 < 0$ if and only if $\frac{1}{2} < \eta < 1$, that is, $\theta > 45^\circ$.

In both cases (λ_1 and λ_2 are complex and λ_1 and λ_2 are real), the ranges of θ such that $|\lambda_1| < 1$ and $|\lambda_2| < 1$ are the same ($\theta > 45^\circ$). Therefore, $|\lambda_1| < 1$ and $|\lambda_2| < 1$ if and only if $\theta > 45^\circ$.

- [1] Y. Fang, M. Gao, J. J. Wylie, and Q. Zhang, *Phys. Rev. E* **77**, 041302 (2008).
 [2] K. L. Schick and A. A. Verveen, *Nature (London)* **251**, 599 (1974).
 [3] G. W. Baxter, R. P. Behringer, T. Fagert, and G. A. Johnson, *Phys. Rev. Lett.* **62**, 2825 (1989).

- [4] X.-I. Wu, K. J. Maloy, A. Hansen, M. Ammi, and D. Bideau, *Phys. Rev. Lett.* **71**, 1363 (1993).
 [5] C. T. Veje and P. Dimon, *Phys. Rev. E* **56**, 4376 (1997).
 [6] C. T. Veje and P. Dimon, *Phys. Rev. E* **54**, 4329 (1996).
 [7] O. Moriyama, N. Kuroiwa, M. Matsushita, and H. Hayakawa, *Phys. Rev. Lett.* **80**, 2833 (1998).

- [8] T. Le Pennec, M. Ammi, J. C. Messenger, and A. Valance, *Eur. Phys. J. B* **7**, 657 (1999).
- [9] E. Longhi, N. Easwar, and N. Menon, *Phys. Rev. Lett.* **89**, 045501 (2002).
- [10] S. Horlück, M. van Hecke, and P. Dimon, *Phys. Rev. E* **67**, 021304 (2003).
- [11] D. Helbing, A. Johansson, J. Mathiesen, M. H. Jensen, and A. Hansen, *Phys. Rev. Lett.* **97**, 168001 (2006).
- [12] A. Mehta and J. M. Luck, *Phys. Rev. Lett.* **65**, 393 (1990).
- [13] J. M. Luck and A. Mehta, *Phys. Rev. E* **48**, 3988 (1993).
- [14] S. McNamara and W. R. Young, *Phys. Fluids A* **4**, 496 (1992).
- [15] J. J. Wylie and Q. Zhang, *Phys. Rev. E* **74**, 011305 (2006).
- [16] R. Yang and J. J. Wylie, *Phys. Rev. E* **82**, 011302 (2010).
- [17] M. Gao, J. J. Wylie, and Q. Zhang, *Commun. Pure Appl. Anal.* **8**, 275(2009).
- [18] O. R. Walton, Lawrence Livermore National Laboratory Report No. UCID-20297-88-1, 1988 (unpublished).
- [19] S. F. Foerster, M. Y. Louge, H. Chang, and Kh. Allia, *Phys. Fluids* **6**, 1108 (1994).
- [20] S. Luding, *Phys. Rev. E* **52**, 4442 (1995).
- [21] N. V. Brilliantov, F. Spahn, J. M. Hertzsch, and T. Poschel, *Phys. Rev. E* **53**, 5382 (1996).